

Improved Measurements of $\bar{B}^0 \rightarrow D^0 \bar{K}^0$ and $\bar{B}^0 \rightarrow D^0 \bar{K}^{*0}$ Branching Fractions

K. Abe,¹⁰ K. Abe,⁴⁶ N. Abe,⁴⁹ I. Adachi,¹⁰ H. Aihara,⁴⁸ M. Akatsu,²⁴ Y. Asano,⁵³
 T. Aso,⁵² V. Aulchenko,² T. Aushev,¹⁴ T. Aziz,⁴⁴ S. Bahinipati,⁶ A. M. Bakich,⁴³
 Y. Ban,³⁶ M. Barbero,⁹ A. Bay,²⁰ I. Bedny,² U. Bitenc,¹⁵ I. Bizjak,¹⁵ S. Blyth,²⁹
 A. Bondar,² A. Bozek,³⁰ M. Bračko,^{22, 15} J. Brodzicka,³⁰ T. E. Browder,⁹ M.-C. Chang,²⁹
 P. Chang,²⁹ Y. Chao,²⁹ A. Chen,²⁶ K.-F. Chen,²⁹ W. T. Chen,²⁶ B. G. Cheon,⁴
 R. Chistov,¹⁴ S.-K. Choi,⁸ Y. Choi,⁴² Y. K. Choi,⁴² A. Chuvikov,³⁷ S. Cole,⁴³
 M. Danilov,¹⁴ M. Dash,⁵⁵ L. Y. Dong,¹² R. Dowd,²³ J. Dragic,²³ A. Drutskoy,⁶
 S. Eidelman,² Y. Enari,²⁴ D. Epifanov,² C. W. Everton,²³ F. Fang,⁹ S. Fratina,¹⁵
 H. Fujii,¹⁰ N. Gabyshev,² A. Garmash,³⁷ T. Gershon,¹⁰ A. Go,²⁶ G. Gokhroo,⁴⁴
 B. Golob,^{21, 15} M. Grosse Perdekamp,³⁸ H. Guler,⁹ J. Haba,¹⁰ F. Handa,⁴⁷ K. Hara,¹⁰
 T. Hara,³⁴ N. C. Hastings,¹⁰ K. Hasuko,³⁸ K. Hayasaka,²⁴ H. Hayashii,²⁵ M. Hazumi,¹⁰
 E. M. Heenan,²³ I. Higuchi,⁴⁷ T. Higuchi,¹⁰ L. Hinz,²⁰ T. Hojo,³⁴ T. Hokuue,²⁴
 Y. Hoshi,⁴⁶ K. Hoshina,⁵¹ S. Hou,²⁶ W.-S. Hou,²⁹ Y. B. Hsiung,²⁹ H.-C. Huang,²⁹
 T. Igaki,²⁴ Y. Igarashi,¹⁰ T. Iijima,²⁴ A. Imoto,²⁵ K. Inami,²⁴ A. Ishikawa,¹⁰ H. Ishino,⁴⁹
 K. Itoh,⁴⁸ R. Itoh,¹⁰ M. Iwamoto,³ M. Iwasaki,⁴⁸ Y. Iwasaki,¹⁰ R. Kagan,¹⁴ H. Kakuno,⁴⁸
 J. H. Kang,⁵⁶ J. S. Kang,¹⁷ P. Kapusta,³⁰ S. U. Kataoka,²⁵ N. Katayama,¹⁰ H. Kawai,³
 H. Kawai,⁴⁸ Y. Kawakami,²⁴ N. Kawamura,¹ T. Kawasaki,³² N. Kent,⁹ H. R. Khan,⁴⁹
 A. Kibayashi,⁴⁹ H. Kichimi,¹⁰ H. J. Kim,¹⁹ H. O. Kim,⁴² Hyunwoo Kim,¹⁷ J. H. Kim,⁴²
 S. K. Kim,⁴¹ T. H. Kim,⁵⁶ K. Kinoshita,⁶ P. Koppenburg,¹⁰ S. Korpar,^{22, 15} P. Križan,^{21, 15}
 P. Krokovny,² R. Kulasiri,⁶ C. C. Kuo,²⁶ H. Kurashiro,⁴⁹ E. Kurihara,³ A. Kusaka,⁴⁸
 A. Kuzmin,² Y.-J. Kwon,⁵⁶ J. S. Lange,⁷ G. Leder,¹³ S. E. Lee,⁴¹ S. H. Lee,⁴¹
 Y.-J. Lee,²⁹ T. Lesiak,³⁰ J. Li,⁴⁰ A. Limosani,²³ S.-W. Lin,²⁹ D. Liventsev,¹⁴
 J. MacNaughton,¹³ G. Majumder,⁴⁴ F. Mandl,¹³ D. Marlow,³⁷ T. Matsuishi,²⁴
 H. Matsumoto,³² S. Matsumoto,⁵ T. Matsumoto,⁵⁰ A. Matyja,³⁰ Y. Mikami,⁴⁷
 W. Mitaroff,¹³ K. Miyabayashi,²⁵ Y. Miyabayashi,²⁴ H. Miyake,³⁴ H. Miyata,³² R. Mizuk,¹⁴
 D. Mohapatra,⁵⁵ G. R. Moloney,²³ G. F. Moorhead,²³ T. Mori,⁴⁹ A. Murakami,³⁹
 T. Nagamine,⁴⁷ Y. Nagasaka,¹¹ T. Nakadaira,⁴⁸ I. Nakamura,¹⁰ E. Nakano,³³ M. Nakao,¹⁰
 H. Nakazawa,¹⁰ Z. Natkaniec,³⁰ K. Neichi,⁴⁶ S. Nishida,¹⁰ O. Nitoh,⁵¹ S. Noguchi,²⁵
 T. Nozaki,¹⁰ A. Ogawa,³⁸ S. Ogawa,⁴⁵ T. Ohshima,²⁴ T. Okabe,²⁴ S. Okuno,¹⁶
 S. L. Olsen,⁹ Y. Onuki,³² W. Ostrowicz,³⁰ H. Ozaki,¹⁰ P. Pakhlov,¹⁴ H. Palka,³⁰
 C. W. Park,⁴² H. Park,¹⁹ K. S. Park,⁴² N. Parslow,⁴³ L. S. Peak,⁴³ M. Pernicka,¹³
 J.-P. Perroud,²⁰ M. Peters,⁹ L. E. Piilonen,⁵⁵ A. Poluektov,² F. J. Ronga,¹⁰ N. Root,²
 M. Rozanska,³⁰ H. Sagawa,¹⁰ M. Saigo,⁴⁷ S. Saitoh,¹⁰ Y. Sakai,¹⁰ H. Sakamoto,¹⁸
 T. R. Sarangi,¹⁰ M. Satapathy,⁵⁴ N. Sato,²⁴ O. Schneider,²⁰ J. Schümann,²⁹ C. Schwanda,¹³
 A. J. Schwartz,⁶ T. Seki,⁵⁰ S. Semenov,¹⁴ K. Senyo,²⁴ Y. Settai,⁵ R. Seuster,⁹
 M. E. Sevior,²³ T. Shibata,³² H. Shibuya,⁴⁵ B. Shwartz,² V. Sidorov,² V. Siegle,³⁸
 J. B. Singh,³⁵ A. Somov,⁶ N. Soni,³⁵ R. Stamen,¹⁰ S. Stanič,^{53,*} M. Starič,¹⁵ A. Sugi,²⁴
 A. Sugiyama,³⁹ K. Sumisawa,³⁴ T. Sumiyoshi,⁵⁰ S. Suzuki,³⁹ S. Y. Suzuki,¹⁰ O. Tajima,¹⁰
 F. Takasaki,¹⁰ K. Tamai,¹⁰ N. Tamura,³² K. Tanabe,⁴⁸ M. Tanaka,¹⁰ G. N. Taylor,²³

Y. Teramoto,³³ X. C. Tian,³⁶ S. Tokuda,²⁴ S. N. Tovey,²³ K. Trabelsi,⁹ T. Tsuboyama,¹⁰ T. Tsukamoto,¹⁰ K. Uchida,⁹ S. Uehara,¹⁰ T. Uglov,¹⁴ K. Ueno,²⁹ Y. Unno,³ S. Uno,¹⁰ Y. Ushiroda,¹⁰ G. Varner,⁹ K. E. Varvell,⁴³ S. Villa,²⁰ C. C. Wang,²⁹ C. H. Wang,²⁸ J. G. Wang,⁵⁵ M.-Z. Wang,²⁹ M. Watanabe,³² Y. Watanabe,⁴⁹ L. Widhalm,¹³ Q. L. Xie,¹² B. D. Yabsley,⁵⁵ A. Yamaguchi,⁴⁷ H. Yamamoto,⁴⁷ S. Yamamoto,⁵⁰ T. Yamanaka,³⁴ Y. Yamashita,³¹ M. Yamauchi,¹⁰ Heyoung Yang,⁴¹ P. Yeh,²⁹ J. Ying,³⁶ K. Yoshida,²⁴ Y. Yuan,¹² Y. Yusa,⁴⁷ H. Yuta,¹ S. L. Zang,¹² C. C. Zhang,¹² J. Zhang,¹⁰ L. M. Zhang,⁴⁰ Z. P. Zhang,⁴⁰ V. Zhilich,² T. Ziegler,³⁷ D. Žontar,^{21,15} and D. Zürcher²⁰

(The Belle Collaboration)

¹*Aomori University, Aomori*

²*Budker Institute of Nuclear Physics, Novosibirsk*

³*Chiba University, Chiba*

⁴*Chonnam National University, Kwangju*

⁵*Chuo University, Tokyo*

⁶*University of Cincinnati, Cincinnati, Ohio 45221*

⁷*University of Frankfurt, Frankfurt*

⁸*Gyeongsang National University, Chinju*

⁹*University of Hawaii, Honolulu, Hawaii 96822*

¹⁰*High Energy Accelerator Research Organization (KEK), Tsukuba*

¹¹*Hiroshima Institute of Technology, Hiroshima*

¹²*Institute of High Energy Physics,
Chinese Academy of Sciences, Beijing*

¹³*Institute of High Energy Physics, Vienna*

¹⁴*Institute for Theoretical and Experimental Physics, Moscow*

¹⁵*J. Stefan Institute, Ljubljana*

¹⁶*Kanagawa University, Yokohama*

¹⁷*Korea University, Seoul*

¹⁸*Kyoto University, Kyoto*

¹⁹*Kyungpook National University, Taegu*

²⁰*Swiss Federal Institute of Technology of Lausanne, EPFL, Lausanne*

²¹*University of Ljubljana, Ljubljana*

²²*University of Maribor, Maribor*

²³*University of Melbourne, Victoria*

²⁴*Nagoya University, Nagoya*

²⁵*Nara Women's University, Nara*

²⁶*National Central University, Chung-li*

²⁷*National Kaohsiung Normal University, Kaohsiung*

²⁸*National United University, Miao Li*

²⁹*Department of Physics, National Taiwan University, Taipei*

³⁰*H. Niewodniczanski Institute of Nuclear Physics, Krakow*

³¹*Nihon Dental College, Niigata*

³²*Niigata University, Niigata*

³³*Osaka City University, Osaka*

³⁴*Osaka University, Osaka*

³⁵*Panjab University, Chandigarh*

³⁶*Peking University, Beijing*

³⁷*Princeton University, Princeton, New Jersey 08545*
³⁸*RIKEN BNL Research Center, Upton, New York 11973*
³⁹*Saga University, Saga*
⁴⁰*University of Science and Technology of China, Hefei*
⁴¹*Seoul National University, Seoul*
⁴²*Sungkyunkwan University, Suwon*
⁴³*University of Sydney, Sydney NSW*
⁴⁴*Tata Institute of Fundamental Research, Bombay*
⁴⁵*Toho University, Funabashi*
⁴⁶*Tohoku Gakuin University, Tagajo*
⁴⁷*Tohoku University, Sendai*
⁴⁸*Department of Physics, University of Tokyo, Tokyo*
⁴⁹*Tokyo Institute of Technology, Tokyo*
⁵⁰*Tokyo Metropolitan University, Tokyo*
⁵¹*Tokyo University of Agriculture and Technology, Tokyo*
⁵²*Toyama National College of Maritime Technology, Toyama*
⁵³*University of Tsukuba, Tsukuba*
⁵⁴*Utkal University, Bhubaneswar*
⁵⁵*Virginia Polytechnic Institute and State University, Blacksburg, Virginia 24061*
⁵⁶*Yonsei University, Seoul*

Abstract

We report on an improved study of $\bar{B}^0 \rightarrow D^{(*)0} \bar{K}^{(*)0}$ decays, based on $274 \times 10^6 B\bar{B}$ events collected with the Belle detector at KEKB. The following branching fractions have been measured: $\mathcal{B}(\bar{B}^0 \rightarrow D^0 \bar{K}^0) = (3.72 \pm 0.65 \pm 0.37) \times 10^{-5}$ and $\mathcal{B}(\bar{B}^0 \rightarrow D^0 \bar{K}^{*0}) = (3.08 \pm 0.56 \pm 0.31) \times 10^{-5}$. We also obtain evidence with 3.2σ significance for $\bar{B}^0 \rightarrow D^{*0} \bar{K}^0$ with $\mathcal{B}(\bar{B}^0 \rightarrow D^{*0} \bar{K}^0) = (3.2^{+1.2}_{-1.1} \pm 0.4) \times 10^{-5}$. No significant signal has been found for the $\bar{B}^0 \rightarrow D^{*0} \bar{K}^{*0}$ and $\bar{B}^0 \rightarrow \bar{D}^{(*)0} \bar{K}^{*0}$ decay modes, and upper limits at 90% CL are presented.

PACS numbers: 13.25.Hw, 14.40.Nd

Within the Standard Model, CP violation arises due to a single phase in the Cabibbo-Kobayashi-Maskawa quark mixing matrix [1]. Measurements of the Unitary Triangle angles therefore test the consistency of the Standard Model. Precise measurements of the branching fractions for $\bar{B}^0 \rightarrow D^0 \bar{K}^{*0}$, $\bar{B}^0 \rightarrow \bar{D}^0 \bar{K}^{*0}$ and $\bar{B}^0 \rightarrow D_{CP}^0 \bar{K}^{*0}$ decays, where D_{CP}^0 denotes D^0 or \bar{D}^0 decay to a CP eigenstate, will allow a measurement of the angle ϕ_3 [2]. The decay $\bar{B}^0 \rightarrow D^0 \bar{K}^0$ can also be used to measure time-dependent CP asymmetry in B decays [3]. The $\bar{B}^0 \rightarrow D^{(*)0} \bar{K}^0$ and $\bar{B}^0 \rightarrow D^{(*)0} \bar{K}^{*0}$ decays have been previously observed by Belle [4]. For all these measurements, knowledge of the ratio of amplitudes $R_{D^0 K^{*0}} = \frac{A(\bar{B}^0 \rightarrow \bar{D}^0 \bar{K}^{*0})}{A(\bar{B}^0 \rightarrow D^0 \bar{K}^{*0})} = \sqrt{\frac{\mathcal{B}(\bar{B}^0 \rightarrow \bar{D}^0 \bar{K}^{*0})}{\mathcal{B}(\bar{B}^0 \rightarrow D^0 \bar{K}^{*0})}}$ is of crucial importance; its value is predicted to be about 0.4 [5].

Here we report improved measurements of $\bar{B}^0 \rightarrow D^{(*)0} \bar{K}^0$ and search for $\bar{B}^0 \rightarrow D^{(*)0} \bar{K}^{*0}$ and $\bar{B}^0 \rightarrow \bar{D}^{(*)0} \bar{K}^{*0}$ [6] decays with the Belle detector [7] at the KEKB asymmetric energy e^+e^- collider [8]. The results are based on a data sample collected at the center-of-mass (CM) energy of the $\Upsilon(4S)$ resonance, which contains 274×10^6 produced $B\bar{B}$ pairs.

The Belle detector is a large-solid-angle magnetic spectrometer that consists of a silicon vertex detector (SVD), a 50-layer central drift chamber (CDC), an array of aerogel threshold Čerenkov counters (ACC), a barrel-like arrangement of time-of-flight scintillation counters (TOF), and an electromagnetic calorimeter (ECL) comprised of CsI(Tl) crystals located inside a superconducting solenoid coil that provides a 1.5 T magnetic field. An iron flux-return located outside of the coil is instrumented to detect K_L^0 mesons and to identify muons (KLM). The detector is described in detail elsewhere [7]. Two different inner detector configurations were used. For the first sample of 152 million $B\bar{B}$ pairs, a 2.0 cm radius beampipe and a 3-layer silicon vertex detector were used; for the latter 122 million $B\bar{B}$ pairs, a 1.5 cm radius beampipe, a 4-layer silicon detector and a small-cell inner drift chamber were used [9].

Charged tracks are selected with a set of requirements based on the average hit residual and impact parameter relative to the interaction point (IP). We also require that the transverse momentum of the tracks be greater than 0.1 GeV/c in order to reduce the low momentum combinatorial background.

For charged particle identification (PID), the combined information from specific ionization in the central drift chamber (dE/dx), time-of-flight scintillation counters (TOF) and aerogel Čerenkov counters (ACC) is used. At large momenta ($> 2.5 \text{ GeV}/c$) only the ACC and dE/dx are used. Charged kaons are selected with PID criteria that have an efficiency of 88%, a pion misidentification probability of 8%, and negligible contamination from protons. All charged tracks having PID consistent with the pion hypothesis that are not identified as electrons are considered as pion candidates.

Neutral kaons are reconstructed via the decay $K_S^0 \rightarrow \pi^+ \pi^-$ with no PID requirements for these pions. The two-pion invariant mass is required to be within $6 \text{ MeV}/c^2$ ($\sim 2.5\sigma$) of the nominal K^0 mass and the displacement of the $\pi^+ \pi^-$ vertex from the IP in the transverse ($r - \phi$) plane is required to be between 0.2 cm and 20 cm. The direction from the IP to the $\pi^+ \pi^-$ vertex is required to agree within 0.2 radians in the $r - \phi$ plane with the combined momentum of the two pions.

A pair of calorimeter showers not associated with charged tracks, with an invariant mass within $15 \text{ MeV}/c^2$ ($\sim 3\sigma$) of the nominal π^0 mass is considered as a π^0 candidate. An energy deposition of at least 30 MeV and a photon-like shape are required for each shower.

\bar{K}^{*0} candidates are reconstructed from $K^- \pi^+$ pairs with an invariant mass within $50 \text{ MeV}/c^2$ (1Γ) of the nominal \bar{K}^{*0} mass. The polarization of \bar{K}^{*0} mesons in B decays

is also utilized to reject background through the use of the helicity angle θ_{K^*} , defined as the angle between the \bar{K}^{*0} momentum in the B meson rest frame and the K^- momentum in the \bar{K}^{*0} rest frame. We require $|\cos(\theta_{K^*})| > 0.3$ for $\bar{B}^0 \rightarrow D^{(*)0} \bar{K}^{*0}$ decay channel. This rejects about 20% of the background and retains 97% of the signal. For the $\bar{B}^0 \rightarrow \bar{D}^{(*)0} \bar{K}^{*0}$ the expected signal to background ratio is worse and we require $|\cos(\theta_{K^*})| > 0.5$.

We reconstruct D^0 mesons in the decay channels: $K^-\pi^+$, $K^-\pi^+\pi^-\pi^+$ and $K^-\pi^+\pi^0$, using requirements that the invariant mass be within $20 \text{ MeV}/c^2$, $15 \text{ MeV}/c^2$ and $25 \text{ MeV}/c^2$ ($\sim 3\sigma$) of the nominal D^0 mass, respectively. In each channel we further define a D^0 mass sideband region, with a width twice that of the signal region and location within $0.1 \text{ GeV}/c^2$ on the nominal D^0 mass. For the π^0 from the $D^0 \rightarrow K^-\pi^+\pi^0$ decay, we require that its momentum in the CM frame be greater than $0.4 \text{ GeV}/c$ in order to reduce combinatorial background. D^{*0} mesons are reconstructed in the $D^{*0} \rightarrow D^0\pi^0$ decay mode. The mass difference between D^{*0} and D^0 candidates is required to be within $4 \text{ MeV}/c^2$ of the expected value ($\sim 4\sigma$).

We combine $D^{(*)0}$ candidates with K_S^0 or \bar{K}^{*0} candidates to form B mesons. Signal events are identified by their CM energy difference, $\Delta E = (\sum_i E_i) - E_b$, and the beam constrained mass, $M_{bc} = \sqrt{E_b^2 - (\sum_i \vec{p}_i)^2}$, where E_b is the beam energy and \vec{p}_i and E_i are the momenta and energies of the B meson decay products in the CM frame. We select events with $M_{bc} > 5.2 \text{ GeV}/c^2$ and $|\Delta E| < 0.2 \text{ GeV}$, and define a B signal region of $5.272 \text{ GeV}/c^2 < M_{bc} < 5.288 \text{ GeV}/c^2$ and $|\Delta E| < 0.03 \text{ GeV}$. In the rare cases where there is more than one candidate in an event, the candidate with the $D^{(*)0}$ and $\bar{K}^{(*)0}$ masses closest to their nominal values is chosen. We use Monte Carlo (MC) simulation to model the response of the detector and determine the efficiency [10].

To suppress the large combinatorial background dominated by the two-jet-like $e^+e^- \rightarrow q\bar{q}$ continuum process, variables that characterize the event topology are used. We require $|\cos \theta_{\text{thr}}| < 0.80$, where θ_{thr} is the angle between the thrust axis of the B candidate and that of the rest of the event. This requirement eliminates 77% of the continuum background and retains 78% of the signal. We also construct a Fisher discriminant, \mathcal{F} , which is based on the production angle of the B candidate, the angle of the B candidate thrust axis with respect to the beam axis, and nine parameters that characterize the momentum flow in the event relative to the B candidate thrust axis in the CM frame [11]. We impose a requirement on \mathcal{F} that rejects 67% of the remaining continuum background and retains 83% of the signal. For the suppressed $\bar{B}^0 \rightarrow \bar{D}^{(*)0} \bar{K}^{*0}$ modes we make a stricter requirement, which has 45% efficiency and 93% background rejection.

Among other B decays, the most serious background comes from $B^0 \rightarrow D^-\pi^+$, $D^- \rightarrow \bar{K}^{(*)0} K^-$, $\bar{K}^{(*)0} K^-\pi^0$, $\bar{K}^{(*)0} K^-\pi^-\pi^+$ and $B^0 \rightarrow D^- K^+$, $D^- \rightarrow \bar{K}^{(*)0} \pi^-$, $\bar{K}^{(*)0} \pi^-\pi^0$, $\bar{K}^{(*)0} \pi^-\pi^-\pi^+$. These decays produce the same final state as the $\bar{B}^0 \rightarrow D^{(*)0} \bar{K}^{*0}$ signal, and their product branching fractions are up to ten times higher than those expected for the signal. To suppress this type of background, we exclude candidates if the invariant mass of the combinations listed above is consistent with the D^- hypothesis within $25 \text{ MeV}/c^2$ ($\sim 3\sigma$). The $\bar{B}^0 \rightarrow D^{*+} K^-$, $D^{*+} \rightarrow D^0\pi^+$ decay can also produce the same final state as the $\bar{B}^0 \rightarrow D^0 \bar{K}^{*0}$ decay; however this decay is kinematically separated from the signal - the invariant mass selection criteria for \bar{K}^{*0} candidates completely eliminates this background. Another potential $B\bar{B}$ background comes from the $\bar{B}^0 \rightarrow D^{(*)0} \rho^0$ decay channel with one pion from the ρ^0 decay misidentified as a kaon. The reconstructed $K^-\pi^+$ invariant mass spectra for these events overlap with the \bar{K}^{*0} signal mass region, while their ΔE distribution is shifted by about $70 \text{ MeV}/c^2$. We study this background using MC simulation. The

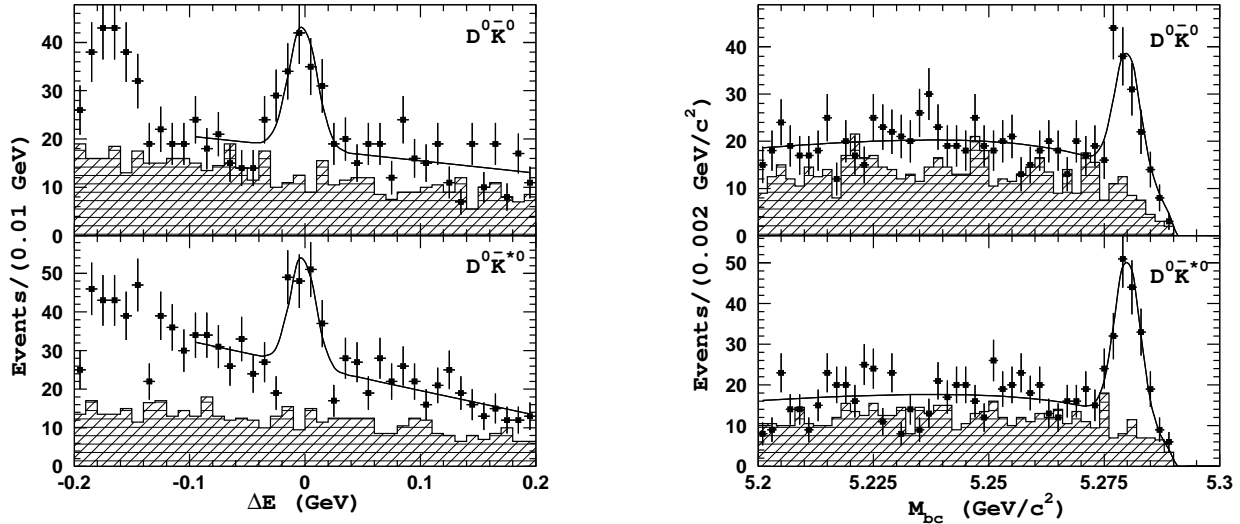


FIG. 1: ΔE (left) and M_{bc} (right) distributions for the $\bar{B}^0 \rightarrow D^0 \bar{K}^{(*)0}$ candidates. Points with errors represent the experimental data, hatched histograms show the D^0 mass sidebands and curves are the results of the fits.

contribution to the $\bar{B}^0 \rightarrow D^{(*)0} \bar{K}^{*0}$ signal region is found to be less than 0.2 events. We examined the possibility that other B meson decay modes might produce backgrounds that peak in the signal region by studying a large MC sample of generic $B\bar{B}$ events. No other peaking backgrounds were found.

The ΔE and M_{bc} distributions for $\bar{B}^0 \rightarrow D^0 \bar{K}^{(*)0}$ candidates are presented in Fig. 1, where all three D^0 decay modes are combined. Each distribution is made for events from the signal region of the other parameter. The hatched histograms in Fig. 1 are the distributions for events in the D^0 mass sideband scaled according to the D^0 mass selection. The sideband shape replicates the background shape well, confirming that the background is mainly combinatorial in nature. Clear signals are observed for the $D^0 \bar{K}^0$ and $D^0 \bar{K}^{*0}$ final states. As a cross check, we also study the K_S^0 candidates' invariant mass and flight distance distributions and \bar{K}^{*0} candidates' invariant mass and helicity distributions for these decays. The distributions mentioned above are shown in Fig. 2, where the points with error bars are the results of fits to the ΔE spectra for data in the corresponding bin, and the histograms are distributions from signal MC. All distributions are consistent with the MC expectations.

For each D^0 decay mode, the ΔE distribution is fitted with a Gaussian for signal and a linear function for background. The Gaussian mean value and width are fixed to the values from MC simulations of the signal. The region $\Delta E < -0.1$ GeV is excluded from the fit to avoid contributions from other B decays, such as $B \rightarrow D^{(*)0} \bar{K}^{(*)0}(\pi)$ where (π) denotes a possible additional pion. For the M_{bc} distribution fit we use the sum of a signal Gaussian and an empirical background function with a kinematic threshold [12], with a shape parameter fixed from the analysis of the off-resonance data. For the calculation of branching fractions, we use the signal yields determined from fits to the ΔE distribution. This minimizes the possible bias from other B meson decays, which tend to peak in M_{bc} but not in ΔE . The fit results are presented in Table I, where the listed efficiencies include intermediate branching fractions. The statistical significance of the signal quoted in Table I is defined as $\sqrt{-2 \ln(\mathcal{L}_0 / \mathcal{L}_{\max})}$, where \mathcal{L}_{\max} and \mathcal{L}_0 denote the maximum likelihood with

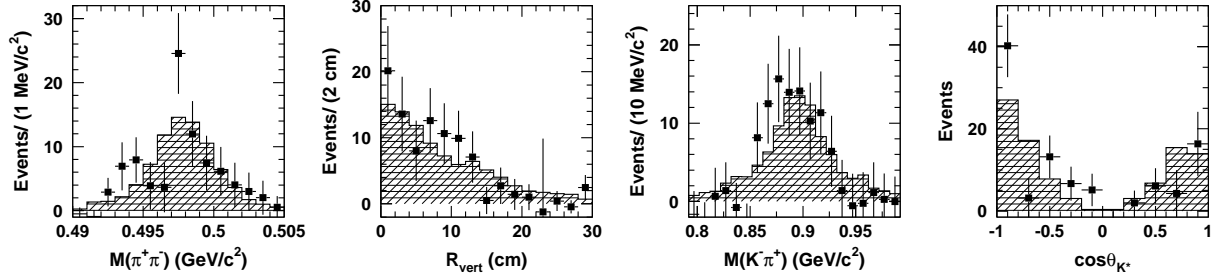


FIG. 2: From left to right: Distributions of invariant mass and flight distance for the K_S^0 candidates' in $\bar{B}^0 \rightarrow D^0 \bar{K}^0$ channel, invariant mass and helicity distributions for the \bar{K}^{*0} candidates' in $\bar{B}^0 \rightarrow D^0 \bar{K}^{*0}$ channel.

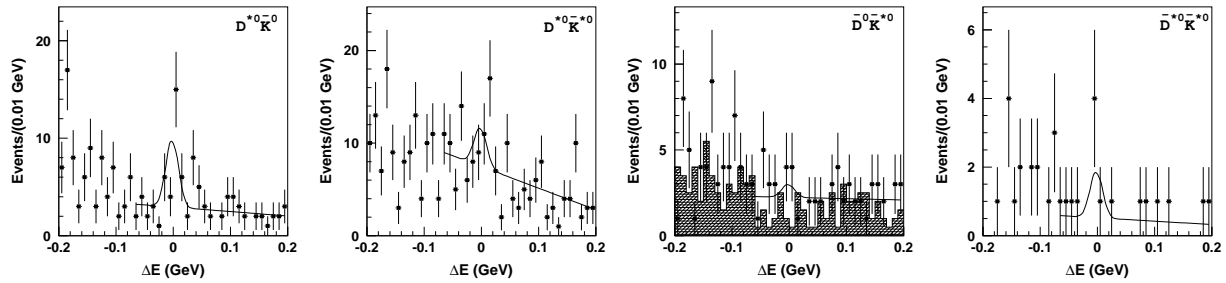


FIG. 3: ΔE distributions for the $\bar{B}^0 \rightarrow D^{*0} \bar{K}^{(*)0}$ and $\bar{B}^0 \rightarrow \bar{D}^{(*)0} \bar{K}^{*0}$ candidates. Points with error bars represent the experimental data, hatched histograms show the D^0 mass sidebands and curves show the results of the fits.

the nominal signal yield and the signal yield fixed at zero, respectively.

For the final result we use a simultaneous fit to the ΔE distributions for the three D^0 decay channels taking into account the corresponding detection efficiencies. The normalization of the background in each D^0 sub-mode is allowed to float while the signal yields are required to satisfy the constraint $N_i = N_{B\bar{B}} \cdot \mathcal{B}(\bar{B}^0 \rightarrow D^{(*)0} \bar{K}^{(*)0}) \cdot \varepsilon_i$, where the branching fraction $\mathcal{B}(\bar{B}^0 \rightarrow D^{(*)0} \bar{K}^{(*)0})$ is a fit parameter; $N_{B\bar{B}}$ is the number of $B\bar{B}$ pairs and ε_i is the efficiency, which includes all intermediate branching fractions.

The statistical significance for $\bar{B}^0 \rightarrow D^{*0} \bar{K}^0$ is 3.2σ . This is the first evidence for this

TABLE I: Fit results, efficiencies, branching fractions and statistical significances for $\bar{B}^0 \rightarrow D^{(*)0} \bar{K}^{(*)0}$ decays.

Mode	ΔE yield	Efficiency (10^{-3})	\mathcal{B} (10^{-5})	Significance
$\bar{B}^0 \rightarrow D^0 \bar{K}^0$	78.1 ± 14.1	8.02	$3.72 \pm 0.65 \pm 0.37$	6.6σ
$\bar{B}^0 \rightarrow D^0 \bar{K}^{*0}$	77.7 ± 14.6	9.98	$3.08 \pm 0.56 \pm 0.31$	6.3σ
$\bar{B}^0 \rightarrow D^{*0} \bar{K}^0$	$19.2^{+6.4}_{-5.8}$	1.97	$3.18^{+1.25}_{-1.12} \pm 0.32$	3.2σ
$\bar{B}^0 \rightarrow D^{*0} \bar{K}^{*0}$	$12.3^{+7.5}_{-7.0}$	2.54	$2.34^{+1.24}_{-1.15} (< 4.8)$ 90% CL	2.1σ
$\bar{B}^0 \rightarrow \bar{D}^0 \bar{K}^{*0}$	$0.4^{+3.6}_{-3.1}$	6.52	< 0.51 90% CL	—
$\bar{B}^0 \rightarrow \bar{D}^{*0} \bar{K}^{*0}$	$3.3^{+2.7}_{-2.1}$	1.72	< 1.9 90% CL	—

decay. We do not observe significant signals for the $\bar{B}^0 \rightarrow D^{*0} \bar{K}^{*0}$ and the $\bar{B}^0 \rightarrow \bar{D}^{(*)0} \bar{K}^{*0}$ decay modes and set 90% CL upper limits for them. Figure 3 shows the ΔE distributions for $\bar{B}^0 \rightarrow D^{*0} \bar{K}^{(*)0}$ and $\bar{B}^0 \rightarrow \bar{D}^{(*)0} \bar{K}^{*0}$ candidates. The upper limit N is calculated from the relation $\int_0^N \mathcal{L}(n)dn = 0.9 \int_0^\infty \mathcal{L}(n)dn$, where $\mathcal{L}(n)$ is the maximum likelihood with the signal yield equal to n . We take into account the systematic uncertainties in these calculations by reducing the detection efficiency by one standard deviation. Using the measured branching fraction for $\bar{B}^0 \rightarrow D^0 \bar{K}^{*0}$ decay and upper limit for $\bar{B}^0 \rightarrow \bar{D}^0 \bar{K}^{*0}$, we set an upper limit on the amplitude ratio: $R_{D^0 \bar{K}^{*0}} < 0.39$.

As a check, we apply a similar procedure to the decay chains with the same final states: $\bar{B}^0 \rightarrow D^+[K_S^0 K^+] \pi^-$ and $\bar{B}^0 \rightarrow D^{*+}[D^0 \pi^+] K^-$. The estimated branching fractions are consistent with the world average values [13].

The following sources of systematic errors are found to be significant: tracking efficiency (1-2% per track), kaon identification efficiency (1%), π^0 efficiency (6%), K_S^0 reconstruction efficiency (6%), efficiency for slow pions from $D^{*0} \rightarrow D^0 \pi^0$ decays (8%), $D^{(*)0}$ branching fraction uncertainties (2% - 6%), signal and background shape parameterization (4%) and MC statistics (2% - 3%). The tracking efficiency error is estimated using η decays to $\gamma\gamma$ and $\pi^+ \pi^- \pi^0$. The kaon identification uncertainty is determined from $D^{*+} \rightarrow D^0 \pi^+$, $D^0 \rightarrow K^- \pi^+$ decays. The π^0 reconstruction uncertainty is obtained using D^0 decays to $K^- \pi^+$ and $K^- \pi^+ \pi^0$. We assume equal production rates for $B^+ B^-$ and $B^0 \bar{B}^0$ pairs and do not include the uncertainty related to this assumption in the total systematic error. The overall systematic uncertainty is found to be 10% for $\bar{B}^0 \rightarrow D^0 \bar{K}^{(*)0}$ and 13% for $\bar{B}^0 \rightarrow D^{*0} \bar{K}^{(*)0}$.

In summary, we report improved measurements of $\bar{B}^0 \rightarrow D^0 \bar{K}^{(*)0}$ branching fractions $\mathcal{B}(\bar{B}^0 \rightarrow D^0 \bar{K}^0) = (3.72 \pm 0.65 \pm 0.37) \times 10^{-5}$ and $\mathcal{B}(\bar{B}^0 \rightarrow D^0 \bar{K}^{*0}) = (3.08 \pm 0.56 \pm 0.31) \times 10^{-5}$. Note that we ignore the possible contribution of $\bar{B}^0 \rightarrow D^0 K^0$ to the former result, since we do not distinguish between \bar{K}^0 and K^0 . We also report the first evidence, with 3.2σ significance for $\bar{B}^0 \rightarrow D^{*0} \bar{K}^0$, with a branching fraction of $\mathcal{B}(\bar{B}^0 \rightarrow D^{*0} \bar{K}^0) = (3.18^{+1.25}_{-1.12} \pm 0.32) \times 10^{-5}$. No significant signal is observed in the $\bar{B}^0 \rightarrow D^{*0} \bar{K}^{*0}$ final state. The corresponding upper limit at the 90% CL is $\mathcal{B}(\bar{B}^0 \rightarrow D^{*0} \bar{K}^{*0}) < 2.34^{+1.24}_{-1.15} \times 10^{-5}$. We also set the 90% CL upper limits for the V_{ub} suppressed $\bar{B}^0 \rightarrow \bar{D}^{(*)0} \bar{K}^{*0}$ decays: $\mathcal{B}(\bar{B}^0 \rightarrow \bar{D}^0 \bar{K}^{*0}) < 0.51 \times 10^{-5}$ and $\mathcal{B}(\bar{B}^0 \rightarrow \bar{D}^{*0} \bar{K}^{*0}) < 1.9 \times 10^{-5}$. The results obtained supersede our previous measurements [4]; these results are consistent with, and more precise than, the previous measurements.

We thank the KEKB group for the excellent operation of the accelerator, the KEK Cryogenics group for the efficient operation of the solenoid, and the KEK computer group and the National Institute of Informatics for valuable computing and Super-SINET network support. We acknowledge support from the Ministry of Education, Culture, Sports, Science, and Technology of Japan and the Japan Society for the Promotion of Science; the Australian Research Council and the Australian Department of Education, Science and Training; the National Science Foundation of China under contract No. 10175071; the Department of Science and Technology of India; the BK21 program of the Ministry of Education of Korea and the CHEP SRC program of the Korea Science and Engineering Foundation; the Polish State Committee for Scientific Research under contract No. 2P03B 01324; the Ministry of Science and Technology of the Russian Federation; the Ministry of Education, Science and Sport of the Republic of Slovenia; the Swiss National Science Foundation; the National Science Council and the Ministry of Education of Taiwan; and the U.S. Department of Energy.

* on leave from Nova Gorica Polytechnic, Nova Gorica

- [1] M. Kobayashi and T. Maskawa, Prog. Theor. Phys. **49**, 652 (1973).
- [2] I. Dunietz, Phys. Lett. **B 270**, 75 (1991).
J.H. Jang, P.Ko, Phys. Rev. **D 58**, 111302 (1998).
- [3] M. Gronau, D. London, Phys. Lett. **B 253**, 483 (1991).
B. Kayser, D. London, Phys. Rev. **D 61**, 116013 (2000).
- [4] Belle Collaboration, P. Krokovny *et al.*, Phys. Rev. Lett. **90**, 141802 (2003).
- [5] M. Gronau Phys. Lett. **B 557**, 198, (2003),
R. Fleischer, Phys. Lett. **B 562**, 234 (2003).
- [6] The inclusion of charge conjugate states is implicit throughout this report. Note that we do not distinguish between final states with \bar{K}^0 and K^0 .
- [7] Belle Collaboration, A. Abashian *et al.*, Nucl. Inst. and Meth. **A 479**, 117 (2002).
- [8] S. Kurokawa and E. Kikutani, Nucl. Instr. and Meth. **A 499**, 1 (2003).
- [9] Y. Ushiroda (Belle SVD2 Group), Nucl. Instr. and Meth. **A 511** 6 (2003).
- [10] R. Brun *et al.*, GEANT 3.21, CERN DD/EE/84-1, 1984.
- [11] CLEO Collaboration, D.M. Asner *et al.*, Phys. Rev. **D 53**, 1039 (1996).
- [12] ARGUS Collaboration, H. Albrecht *et al.*, Phys. Lett. **B 241**, 278 (1990).
- [13] S. Eidelman *et al.* (Particle Data Group), Phys. Lett. **B 592**, 1 (2004).